A Simple Low-Cost Shared-Aperture Dual-Band Dual-Polarized High Gain Antenna for Synthetic Aperture Radars

F. Qin, S.Gao, *Member, IEEE,* Q.Luo, *Member, IEEE,* C. Mao, C.Gu,
G. Wei, J. Xu, J. Li, C. Wu, K. Zheng and S. Zheng, *Member, IEEE*

***Abstract*—This paper proposes a novel shared-aperture dual-band dual-polarized high-gain antenna for applications in synthetic aperture radars (SAR). One critical challenge in the design of high-gain SAR antenna is the feed network which is usually complicated, bulky, heavy and lossy, in particular if the SAR system is required to operate at multiple frequency bands and orthogonal polarizations, as a number of large-size, lossy feed networks at multiple layers are needed to cover all the frequency bands and each polarization, respectively. To reduce the complexity and cost of SAR antennas, a dual-band dual-polarized high-gain Fabry-Perot (FP) resonate antenna is designed and applied to shared-aperture SAR antenna application for the 1st time. A novel double-layer FSS is proposed as the Partially Reflective Surface (PRS) for the FP resonate cavity with realized dual-band performance. The units of this double-layer FSS are a quasi-star patch and a square slot printed on the upper- and lower-layer substrate, respectively. The resonate frequency (full reflection) and 'zero' reflection magnitude of this proposed quasi-star patch can be controlled by adjusting its parameters easily, which leads to high flexibility for deigning dual-band FP antennas. A novel dual-band dual-polarized feed source for FP antenna is also proposed by using a compact sparse array at higher band interleaved with one radiating element at lower band. To verify the concept, a C/X dual-band dual-polarized SAR antenna is designed and a prototype is developed and measured. Measured results have a good agreement with the simulated ones, which shows that a peak gain of 16.3 dBi and 19.8 dBi is obtained at lower- and upper-bands, respectively. High isolation (>25 dB) is also achieved at both bands. Compared to traditional dual-band dual-polarized SAR antennas with high gain, the proposed antenna has achieved a significant reduction in the complexity, mass, loss and cost of the feed network, which is particularly important for space-borne SAR systems.**

***Index Terms*—antenna, SAR antenna, Dual-band, dual-polarization, high gain, Fabry-Perot**

I. INTRODUCTION

THE IMPORTANCE of radar observations for civilian remote sensing and Earth observation has increased considerably in the last decade, which motives the development of synthetic aperture radar (SAR). As a key component in SAR system, the antenna is required to operate at multiple frequency bands and dual polarizations with high isolation between orthogonal polarization ports [1]. Multi-band operation can provide finer resolution scanning, better penetration and reflection data from various scatters. Dual-polarized antenna is a good solution to enhance the information content as it can provide both of co-polar and cross-polar scattering data. SAR antenna is usually a bulky, heavy and expensive component in the SAR systems. For space-borne SAR system, it is critical to reduce the complexity, size, mass and cost of SAR antenna while achieving the capability of multi-band operation, dual polarizations and high gain. These are conflicting requirements in current SAR antennas, unfortunately.

Dual-band dual-polarized (DBDP) antenna arrays have been used in many space-borne SAR systems. For instance, in the shuttle imaging radar (SIR-C) system [2], two frequencies (L-band and C-band) and dual-polarization were used; however, the L-band and C-band antennas did not share the same aperture, which resulted in large and bulky structure and would not be compatible with currently operated space platforms. In practice, it is desirable to design a single antenna which can integrate with a spacecraft using minimum size and cost. Due to this reason, shared-aperture dual-band dual-polarized antenna for future SAR applications becomes an attractive and promising topic [3-9]. One of the most popular techniques for designing the share-aperture DBDP antennas is using a perforated structure. L band microstrip patches operating at 1.275 GHz and C band patches operating at 5.3 GHz were integrated in one aperture with a frequency ratio of 4.16:1 [3]. The cross polarization levels below -25 dB were obtained with 100-MHz bandwidth at each band in this design. Another example was reported in [4]. In order to share the same aperture, a 2×2 L-band elements were integrated with an array of 12×16 X-band elements to meet the requirement of shared-aperture. Interlaced layout is another way for designs of aperture-shared DBDP antennas. An example was reported in [5], where interlaced patches with diploes were designed. This antenna operated at S- and X-bands and achieved an isolation (between two polarizations) over 22 dB for both bands. Although these shared-aperture SAR antennas can achieve high gain and high isolation between polarization ports at each frequency band, it is very challenging to design the feed network of SAR antennas. Usually a number of large-size feed networks at multiple layers

F.Qin, G.Wei, J. Xu, J. Li, C.Wu. K.Zheng are with School of Electronics and Information, Northwestern Polythechnical University, Xi'an 710072, China. F.Qin is also with School of Engineering and Digital Arts, University of Kent, Canterbury, CT2 7NT, (email address: f.qin@kent.ac.uk)

S.Gao, Q.Luo, C.Mao, G.Cao are with School of Engineering and Digital Arts, University of Kent, Canterbury, CT2 7NT, UK. (email: s.gao@kent.ac.uk)

S.Zheng is with National Key Laboratory of Antennas and Microwave Technology, Xidian University, Xi'an 710071, China

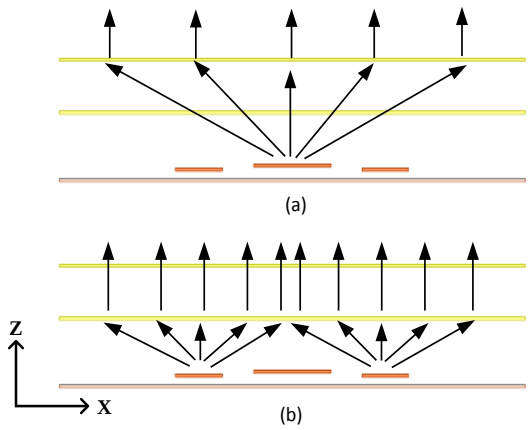

Fig.1. Principle of Dual-band operation: (a) operating at lower band; (b) operating at higher band

are required for one multi-band dual-polar. SAR antenna, as a separate feed network, is needed for operation at a single polarization at each frequency band, which causes high complexity, bulky size, high mass and high fabrication cost of SAR antennas. Also it is difficult to accommodate these feed networks due to their bulky sizes and limited space available between antenna elements. The mutual coupling amongst these feed networks and the antenna elements cause deterioration of the antenna performance, thus these mutual coupling effects need to be minimized during the SAR antenna designs which makes the SAR antenna design a very challenging task. In addition, to achieve efficient coupling from the feed network to specific feed port, it usually requires a large number of vias or blind vias for inter-connections amongst different layers which leads to complexity and high cost of fabrication. For SAR applications, especially in low-cost small satellites [10], a simple, low-cost shared-aperture dual-band dual-polarized high-gain SAR antenna is required. The objective of this work is to fill this gap.

This paper presents our work on the design of a DBDP shared-aperture antenna with high gain and simple feed structure and low cost for SAR applications. To reduce the complexity and size of feed networks in SAR antennas, the concept of Fabry-Perot (FP) cavity antenna is employed here. A FP antenna generally comprises a simple primary source placed in the cavity formed between a partially reflective surface (PRS) and a fully reflective ground plane [11]. When the space between these two plates is about integer times of half wavelength, the forward radiation can be enhanced remarkable by means of in-phase bouncing. Studies on Frequency Selective Surface (FSS) structures promote the development of FP antennas in recent years. Most of 2-D FP resonate antennas are based on FSS [12-15], which also behave as PRS at the antenna operating frequencies. The advantages of FSS are simplicity, low cost, ease of fabrication and mounting. It is also easy to change their properties, such as the reflection magnitude and phase, by optimizing the parameters of the FSS. FP antennas attracted lots of attentions and they have been deployed in several wireless communication systems and radar applications in recent decades due to its promising advantages.

Many FP antennas have been reported, including dual-band FP antennas. For instance, an electromagnetic band gap (EBG) superstrate consisting of triple-layer dielectric cylindrical rods was employed in one dual-band design [16]. Two operating bands were obtained by the insertion of defect rods in the EBG structure. However, this design needs a 3-D EBG structure, which complicates its fabrication. Another method of realizing dual-band is based on the inverted reflection phase gradient of PRS. A dual-band FP antenna using single-resonant and single layer PRS was reported in [17]. This work used the positive gradient of the reflection phase versus frequency curve of the PRS occurred around the resonate frequency to satisfy the resonate condition at two frequencies. Similar design was reported in [18], two plain unprinted identical dielectric slabs were applied to generate the inverted reflection phase gradient of PRS. One drawback of this method is that it cannot control the two frequencies independently. When the lower frequency is changed, the upper frequency is changed as well. Moreover, designing two frequencies with a large frequency ratio using this method is difficult. The concept of artificial magnetic conductor (AMC) can be applied as the ground plane instead of a metal ground plane to achieve dual-band characteristics [19]. Only one layer PRS is needed using this method. However, an additional AMC has to be designed, which increases antenna's complexity. More importantly, it is difficult to print the feed network on the same substrate with AMC if a small array is needed as the primary source. Another method for dual-band FP antennas is to use a double-layer FSS superstrate as the PRS. The cavity height and distance between the two layers are appropriately selected, two separated FP resonate cavities are formed and dual-band operation is expected using this method. For instance, a double-layer of the same printed dipoles were introduced as the PRS to enhance the gain of a microstrip patch antenna at two bands with orthogonal linear polarization [20]. In this antenna, the lower and upper bands were designed as vertical and horizontal polarization, respectively. However, it cannot achieve dual-polarizations at both bands due to the asymmetrical structure of the dipoles printed in each layer.

This paper reports the detailed design and implementation of a simple, low-cost shared-aperture dual-band dual-polarized high-gain SAR antenna. Compared to conventional multi-band dual-polarized SAR antennas, it achieves a significant reduction in complexity, mass and fabrication cost. FP antenna is applied to designs of shared-aperture dual-band dual-polarized high-gain SAR antenna. The method of double-layer FSSs creating each band separately is used in this paper. We choose this method is due to the reason that it can control the two frequencies separately. Thus two typical frequencies (5.3 GHz and 9.6 GHz) used in SAR application with large frequency ratio (1.8:1) can be achieved. There is also no AMC needed in this design. Hence we can design the dual-band dual-polarized feed network on one side of ground plane. In our design, the FSSs printed on the upper- and lower-layer are a quasi-star patch and a square loop, respectively. A characteristics of this quasi-star patch is that it can easily control the full and 'zero' reflection magnitude by adjusting its outline size and small-arms' sizes. This characteristic is very important and useful for designing dual-band FP antennas. A single slot-

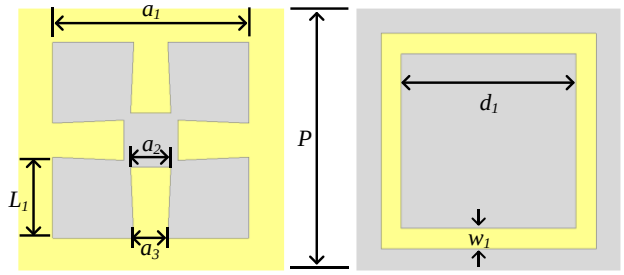

(a) (b)

Fig.2. Unit cell of two-layer PRS: (a) upper layer; (b) lower layer

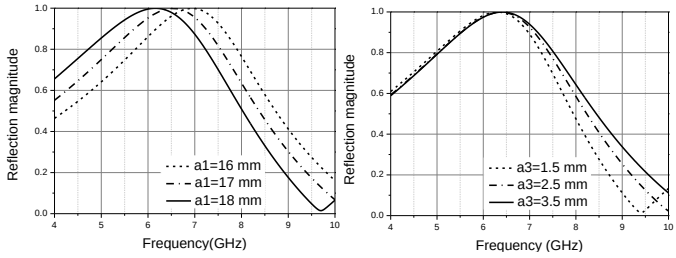

(a) (b)

Fig.3. Reflection magnitude of the upper-FSS

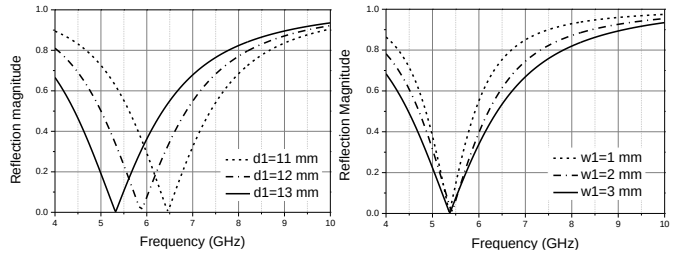

(a) (b)

Fig.4. Transmission magnitude of the lower-FSS

coupled patch antenna [21, 22] operating at C band is employed as the lower frequency feed antenna. This C-band patch is surrounded by a 2×2 sparse feed array operating at X band. All of the feed antennas are fed by two orthogonal ports to generate dual-polarizations. All the design is implemented with the EM software CST Microwave Studio. To validate the concept, a prototype is fabricated and measured.

This paper is organized as follows: In section II, details of the structure of PRS are given, and the antenna design methods are also explained. In section III, the analysis of parameters is reported. The simulation and measurement results are shown in section IV. Finally, a conclusion is given in section V.

II. Dual-Band PRS Design

A. Principle of Dual-band Operation

An analysis of FP antenna can be realized using ray theory. According to the analysis in [11], the maximum directivity occurs at broadside when the equation (1) is satisfied,

$$\varphi_H+\varphi_L-2\pi/\lambda\times 2h=2k\pi,\ k=\pm0,\pm1,\pm2 \qquad (1)$$

where φ_H and φ_L are the reflection phase of PRS and ground plane, respectively. h is the distance between the PRS and the ground plane. The directivity enhancement contributed by the PRS is theoretically

$$D_e=(1+R)/(1-R) \qquad (2)$$

where R is the magnitude of the PRS reflection coefficient. When a PEC ground plane is applied ($\varphi_L=\pi$), (1) can be rearranged as

$$\varphi_H=4\pi h/c\times f+(2k-1)\pi,\ k=0,\pm1,\pm2 \qquad (3)$$

The principle of obtaining dual-band performance relies on engineering the reflection phase of the PRS to achieve resonate conditions at two frequencies. Based on this principle, double-layer FSS is needed as shown in Fig.1. The upper- and lower FSS form a FP resonate cavity with ground plane operating at lower- and upper-band, respectively. Each FSS also should have frequency selection performance: when this antenna is working at lower frequency, namely the FP cavity formed by upper-FSS and GND, the lower-FSS should act as free space and let the electromagnetic wave go through it freely at lower frequency, as shown in Fig.1 (a). When this antenna is working at upper band, the upper-FSS should allow higher frequency electromagnetic wave go through freely, as shown in Fig.1 (b). It also should be noted that this double-FSS layer not only needs frequency selection performance but also enough large reflection magnitude at the frequency each band is operating according to equation (2). In brief, in order to design the dual-band FP antenna, the upper-FSS needs high reflection magnitude and band-pass performance at lower and upper frequencies. The lower-FSS needs band-pass and high reflection magnitude performance at lower and upper frequencies.

B. Design of FSS

FSSs have two kinds of metallic patterns: one is patch type, such as dipole and loop. They are designed to reflect the electromagnetic wave at its resonate frequency. The other is slot type, which is a complementary structure of patch-type FSS, such as grid lattice and square slot. This type has the band-pass performance at its resonate frequency. In our proposed antenna, a patch-type and a slot-type FSSs are designed to be the upper- and lower-layer of the double-layer FSS, respectively.

A novel patch-type FSS is studied to act as upper-layer FSS. The configuration of this FSS is shown in Fig.2 (a). It is a quasi-star patch with the period of P. The colors of gray and yellow are the copper conductor and substrate, respectively. Four small arms are connected and placed around a square patch printed in the center on the substrate. The dimension of the outline of this FSS is $a_1\times a_1$. The size of the center square patch is $a_2\times a_2$ and the length of the outside of the arms is L_1. The space between the two arms is set as a_3. The reflection coefficient of this FSS is investigated and plotted in Fig.3. It shows that a 'zero' reflection magnitude occurs at upper frequency with a high reflection magnitude at lower frequency. The dimension of outline (a_1) mainly determines the resonate frequency as shown in Fig.3 (a). The resonate frequency changes from 7.0 GHz to 6.0 GHz with the variation of a_1 from 16 mm to 18 mm. The 'zero' reflection magnitude at upper frequency is decided by the parameter of (a_3) as show in Fig.3 (b). There is little influence on the resonate frequency when a_3 is changed. But the 'zero' reflection magnitude moves to lower frequency as a_3 increases. It can be found that this quasi-star patch allows to control the

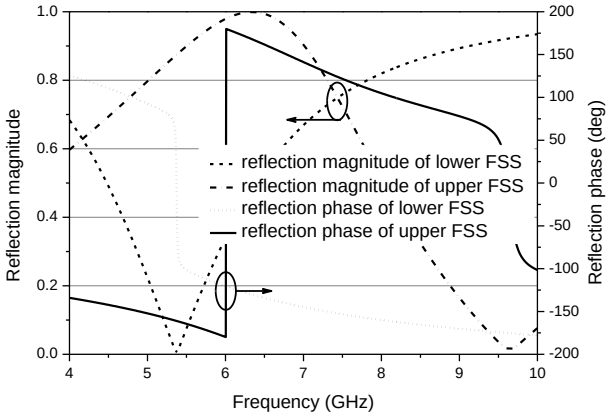

Fig.5. Reflection coefficient of the two-layer FSSs

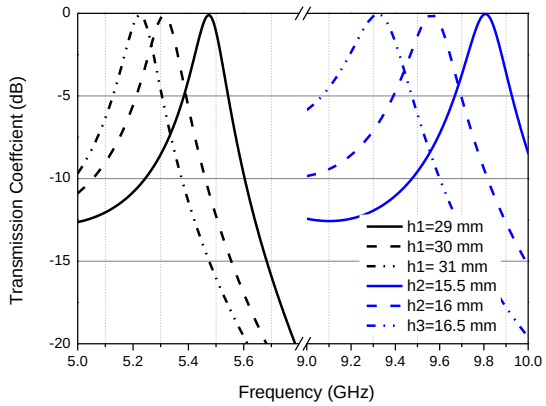

Fig.6. The transmission using image theory

high reflection magnitude at lower band and 'zero' reflection magnitude at higher band easily by adjusting the values of a_2 and a_3. This means that the specific reflection or transmission magnitude of this proposed FSS at specific frequencies can be obtained by changing these parameters. This characteristic is quite important and useful for the design of lower-band in the dual-band FP antennas.

A simple square slot is designed for lower-FSS as shown in Fig.2 (b). The width and the inner length of this slot are set as w_1 and d_1. As the slot has band-pass performance, the transmission coefficient instead of reflection coefficient is studied in Fig.4. It can be observed that the resonate frequency is mainly controlled by the length of the slot as shown in Fig.4 (a). The resonate frequency moves to lower frequency with the increase of d_1. There is little influence on the resonate frequency when the width of slot is varied. However, this parameter influences the bandwidth of band-pass. The reflection magnitude decreases with the increase of w_1 at upper band as shown in Fig.4 (b), which can be used to adjust the reflection magnitude at X-band.

Fig.5 shows the optimized results of reflection coefficient of these two FSSs structures. The reflection magnitude of the quasi-star FSS is around 0.9 at 5.3 GHz with the value below 0.1 at 9.6 GHz, which means a high reflection and transmission are obtained in lower and higher frequencies, respectively. At the same time, these values are around 0.85 at 9.6 GHz and below 0.1 at 5.3 GHz. The reflection phase of each FSS layer is also calculated, which can be used to estimate the cavity height for each band based on the equation (1).

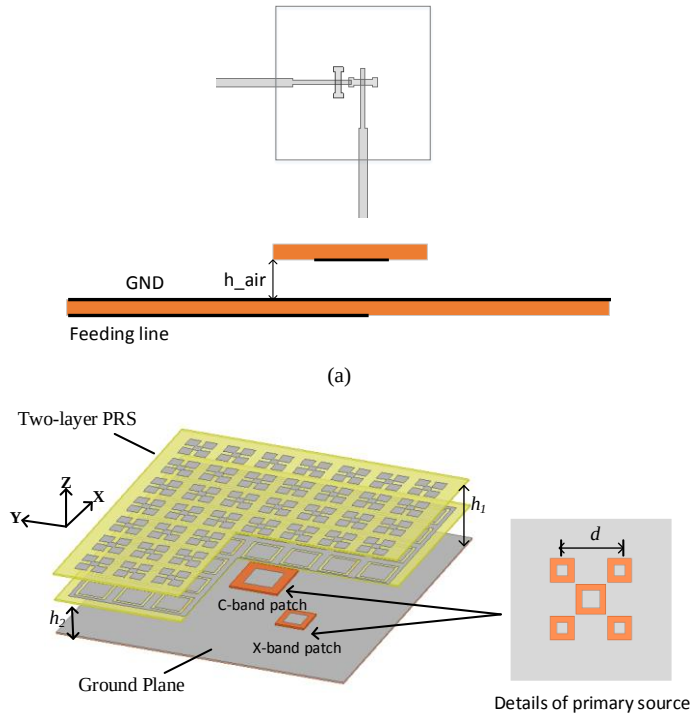

Fig.7. (a) the structure of coupled patch; (b) the overall structure of the proposed antenna

In order to check the possibility of dual-band performance using the double-layer FSS as the PRS, the computation of the transmission coefficient using image theory is carried out. Image theory is done by eliminating the ground and adding its image on the other side. According to the image theory, there should exist total transmission coefficient at resonate frequency when such a structure is held above the ground plane. It can be seen that the transmission coefficient through the cavity is close to 0 dB at the frequencies of the FP cavity resonance as shown in Fig.6. As the height of cavity increases, these two resonate frequencies move to lower frequencies, which have a good agreement with the equation (2). Thus, the resonate frequencies can also be tuned by adjusting the height of the cavity. The high transmission is entirely due to FP cavity resonance. The cavity efficiently radiates with a narrow beam, forming a high-directivity FP resonate antenna at these frequencies.

III. Dual-Band Dual-Polarized High Gain Antenna

A. Antenna Configuration

The overall antenna structure is shown in Fig.7. The proposed PRS consisting of the double-layer FSS designed in Section II is mounted above the ground plane with the cavity height of h_1 and h_2.

As an integral part of the resonator antenna, the feed antenna plays an important role on antenna's performance. Several types of antennas have been reported as the excitation of the FP antenna, such as patches and dipoles. In this design, slot coupled patch antenna is chosen and a novel feed antenna using

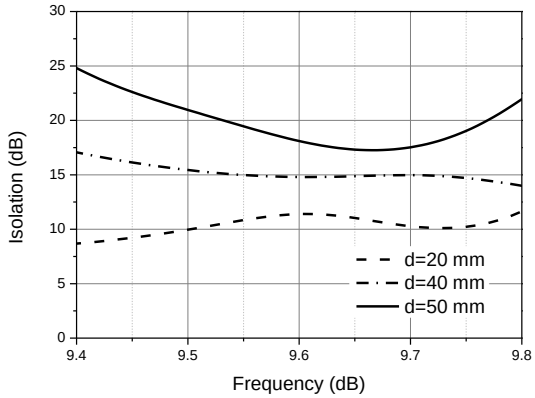

Fig.8. Isolation between inter-elements in FP cavity

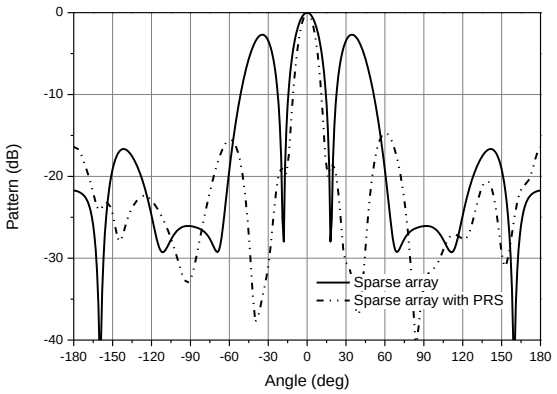

Fig.9. Normalized Radiation patterns of spare array: with and without PRS

a compact-size sparse array at higher band interleaved with one radiating element at lower band is proposed and designed in this FP antenna due to its low profile, easy feeding and stable broadside radiation. Using slot coupled patch antenna allows to print the feed network on the other side of the GND, which provides more space and flexibility to design the feed network. The structure of the slot-coupled patch antenna is shown in Fig.7 (a). The patch is coupled with the feed line through two orthogonal 'H' slots in the ground plane. The patch is spaced from the GND by an air-gap. A simple matching network is etched on the bottom layer to make the antenna provide a wide impedance bandwidth. The whole geometry of the feed antennas is constructed as shown in Fig.7 (b). A C-band patch is placed in the center of the ground plane. A 2×2 antenna array operating at X band is placed around the C-band patch. The space between the X-band elements is set as *d*. The feed network is printed on the other side of the substrate. There are four ports for H-pol and V-pol at two frequency bands in this feed network. The X-band radiating elements are fed with signals with 180^o phase differences, contributing to further improvement of the cross-polarization levels.

B. Performance of Proposed Antenna at X band

As described above, a 2×2 antenna array operating at X band is employed as the primary source. It is necessary to analysis how the inter-element isolation and radiation characteristics depend on the inter-element space. It can be expected that the inter-element isolation in resonator cavity tends to be lower than conventional antenna arrays because the EM-wave produced by any of the array elements can be reflected from the

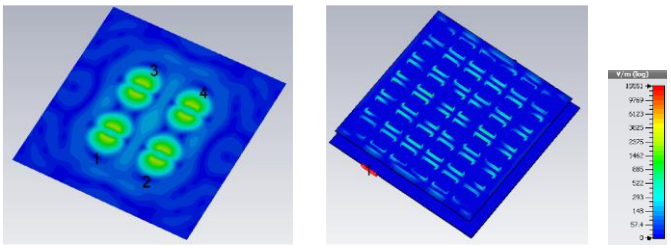

Fig.10. E-field: (a) sparse patch array; (b) surface of PRS fed by spare array

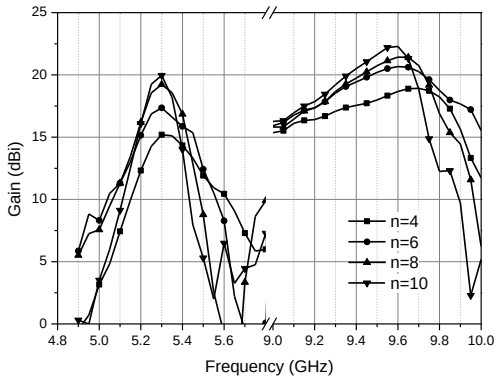

Fig.11. Gain with different number of units at both bands

PRS and in turn received by any adjacent array element. In order to study the isolation between the inter-elements, two single-polarized elements placed in the FP resonate cavity were simulated with the variation of *d*. The dimension of PRS is chosen as 140×140 mm consisting of 6×6 PRS units. Fig.8 shows the isolation of slot-coupled elements in the resonate cavity. It monotonically increases as the inter-element distance *d* increases for a given dimension of PRS. The isolation is below 12.5 dB when the space is 20 mm. This values drops to around 15 dB with d=40 mm. The isolation keeps increasing as *d* increases.

The space between inter-elements should be enough large according to the analysis in order to obtain an acceptable isolation. Here, *d*=50 mm (1.6λ_0 at 9.6 GHz) is chosen. In this case, the X-band feed array can be seen as a sparse array. It is unrealistic in practice using such a sparse array due to high sidelobe level (SLL) caused by the large space. While, when the proposed PRS is added, not only directivity but also SLL of the sparse array can be improved [23]. A comparison of normalized radiation patterns between the sparse array and the one with PRS is investigated in Fig.9. It can be found that the SLL of sparse array without PRS is only -3dB. A great improvement of the SLL is obtained when the PRS is applied, whose value decrease to around -15dB.

This phenomenon can be explained by the E-field distribution of the spare array with and without PRS shown in Fig.10. For the spare array, the strongest E-field occurs on the surface of each patch. Due to the large space between each element, it is difficult to form a uniform E-filed distribution on the effective aperture, resulting in a large SLL. When the PRS is employed, the phase and amplitude of E-filed become uniform on the surface of PRS at the resonate condition. In this case, the radiation patterns of spare array with PRS are generated by the PRS with uniform E-filed instead of the spare array itself. That is why a great improvement including directivity and SLL is obtained when a PRS is applied.

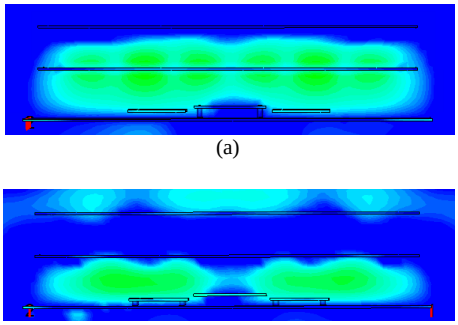

(a) (b)

Fig.12. E-filed in the cavity; (a) 5.3 GHz; (b) 9.6 GHz

C. Effect of physical size on antenna's Gain

FP antenna can be considered as a leaky wave antenna where the leaky wave propagate toward the edges of PRS and produce radiating current distribution on the surface of PRS. Increasing the dimension of PRS means larger radiating aperture, which can lead to higher directivity. Meanwhile, a smaller size is preferable in the application of space-borne SAR. In this section, the study on the PRS size is carried out. Fig.11 illustrates the calculated gain as a function of frequency with different numbers of PRS units, where the dimension of PRS varies from 80×80 mm^2 (4×4 units) to 200×200 mm^2 (10×10 units). In order to study the effects more suitably, the gain is absolute gain in the broadside direction and the loss caused by impedance mismatching is not included. It is revealed from Fig.11 that the gain increases with an increasing number of PRS units, which agrees with our expectation. A peak gain of 15.2 dBi and 18.9 dBi occurs at C- and X-band, respectively, when 4×4 PRS units are used. Then it increases by 2.1 dB, 4 dB and 4.7 dB when the number of PRS units increases to 6×6, 8×8 and 10×10 at C band. This value is increased by 1.8 dB, 2.5 dB and 3.2 dB at X band, respectively. The simulation results simultaneous show that enhancing the dimension of PRS more than 8×8 units has a little enhancement on the gain at these two bands. This is because the dimensions of the PRS substrate layer is big enough and the reflected wave from the edges of PRS has little contribution to antenna's gain. In addition, it can affect 3-dB gain bandwidth after a certain size of PRS although a higher gain is possible. It is due to the reason that during the design of the PRS, it is assumed that the PRS has a normal incident angle. It gives a good approximation if the size of the PRS is moderate compared to the height of the cavity, so the incident angle effect can be ignored. However, with larger size of the PRS, the angle of the incident wave cannot be ignored otherwise phase errors can affect the overall radiation pattern and cause the decrease of 3-dB gain bandwidth.

IV. Simulation and Measurement

In this section, a finite-size antenna structure has been simulated based on the optimized designs obtained in the previous section. Measurements of a prototype of the proposed double-layer DBDP FP antenna are also presented.

The structure has been formed using the optimized double-layer FSS as the proposed PRS placed in front of a ground plane. The feed antennas are located in the FP cavity sharing the same aperture. The space between each radiating element in X-band feed array is chosen as 50 mm, which has shown high isolation. The feed antennas and network are etched on the

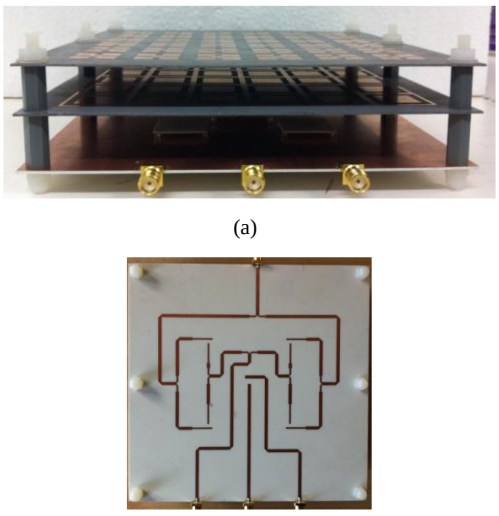

(a) (b)

Fig.13 (a) photograph of the fabricated DBDP FP antenna; (b) feed network of the proposed antenna

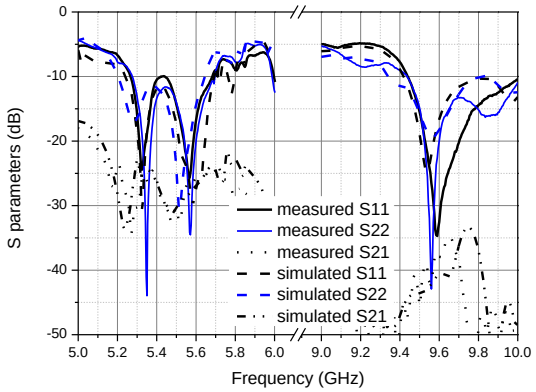

Fig.14. S parameters of the proposed antenna

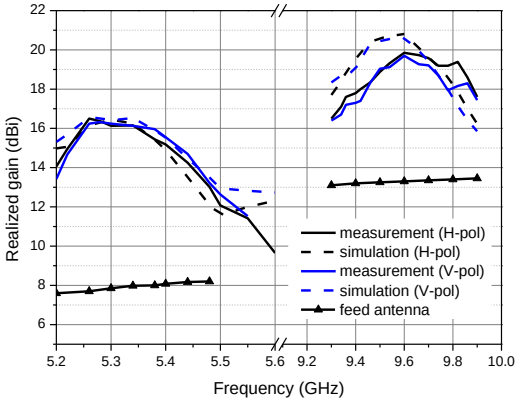

Fig.15. Realized gain of the proposed antenna

substrate of Rogers 4003C (ε_r=3.55) with the thickness of 0.8 mm. A finite lateral size of the double layer FSS with dimension of 140×140 mm^2 (6×6 units) is chosen, which is about 2.5 λ at 5.3 GHz and 4.5 λ at 9.6 GHz, respectively. Although a larger dimension can lead to higher gain, a smaller size and better 3-dB bandwidth is more desirable in practice application. The heights of the dual-band cavities, h_1 and h_2, are optimized to 31 mm and 10.8 mm, respectively. This double-layer PRS is made from 0.787 mm Rogers 5880 (ε_r=2.2) and it is held by six hexagonal nylon spacers placed around the corners of ground plane to support the suspended PRS layer and create the depth

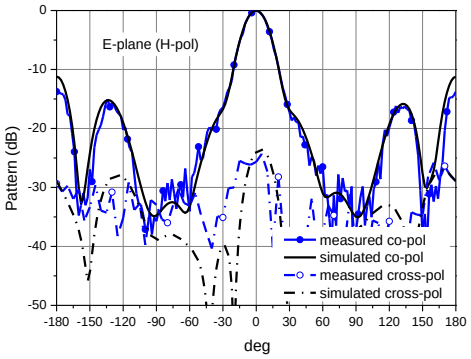

(a)

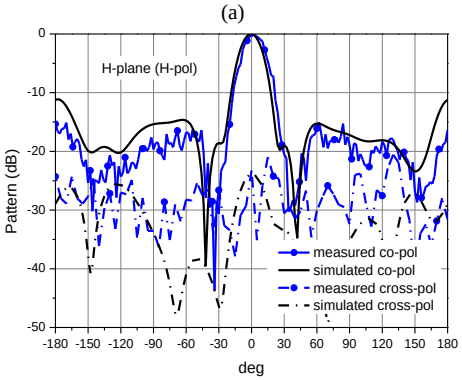

(b)

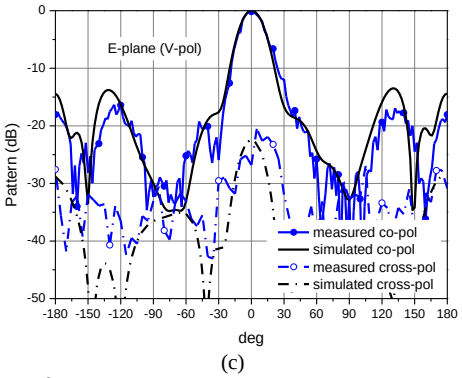

(c)

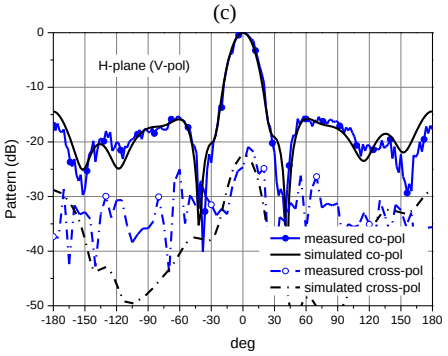

(d)

Fig.16. Measured rediation patterns at 5.3 GHz: (a) H-pol in E-plane; (b) H-pol in H-plane; (c) V-pol in E-plane; (d) V-pol in H-plane

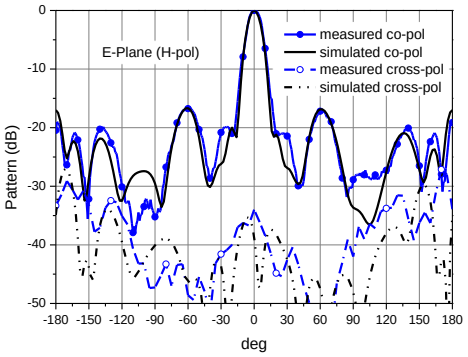

(a)

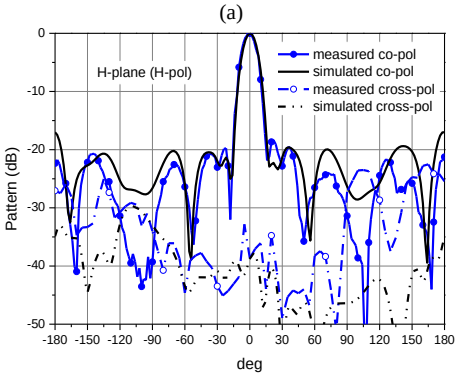

(b)

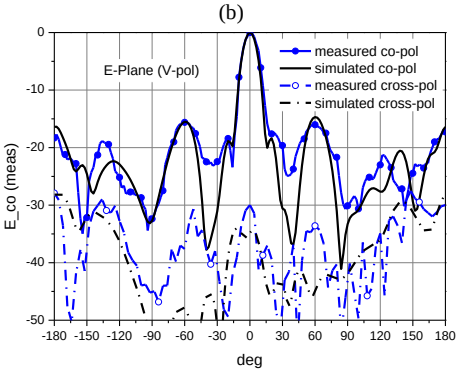

(c)

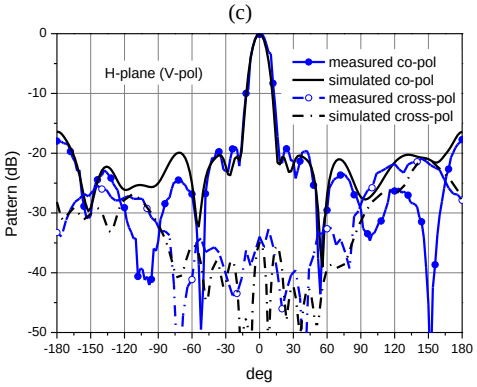

(d)

Fig.17. Measured rediation patterns at 5.3 GHz: (a) H-pol in E-plane; (b) H-pol in H-plane; (c) V-pol in E-plane; (d) V-pol in H-plane

of the air cavity. They are also modeled and taken into account in the numerical simulation.

An analysis of the E- field distributions in the FP resonate cavity is carried out to better understand the radiation mechanism of this antenna shown in Fig.12. As our expect, when this antenna is working at 5.3 GHz, the resonate cavity is formed by the top layer of PRS and ground plane. The bottom layer acts like free space for E-filed in this case. When this antenna is working at 9.6 GHz, the bottom layer of PRS and the ground plane forms a FP resonate cavity to enhance the gain and the E-filed can spread through the upper frequency freely.

The pictures of a prototype are shown in Fig.13. The simulated and measured S parameters of this proposed antenna

are shown in Fig.14. At C band, the 10-dB return-loss for H-polarization is from 5.25 GHz to 5.65 GHz from the simulated results and 5.28 GHz to 5.64 GHz from the measured results. For V-polarization, this value is from 5.2 GHz to 5.63 GHz and 5.28 GHz to 5.63 GHz, respectively. At X band, the simulated 10-dB return-loss is wider than 600 MHz from 9.4 GHz for both polarizations. The measured results have a good agreement with the simulated values. Due to the orthogonal 'T' construction of coupled slots, a good isolation is achieved, which is better than 25 dB and 35 dB at lower- and upper-band, respectively.

Fig.15 indicates the simulated and measured realized gain of this antenna. The measured gain is found by the gain comparison method, using a standard gain horn antenna with known gain. It is illustrated that the realized gain at X band is higher than the one at C band as the electrical aperture of upper frequency is larger than the one of lower band. The measured peak gain occurs at 5.34 GHz in H-pol and 5.28 GHz in V-pol, reaching 16.2 dBi and 16.3 dBi, respectively. At X band, both of the peak gain in dual-polarizations occur at 9.6 GHz, which are 19.8 dBi in H-pol and 19.7 dBi in V-pol, respectively. Compared to the results, around 1 dB gain loss occurring at X band is attributed to fabrication tolerances. The 3-dB gain bandwidth is from 5.22 GHz to 5.45 GHz (4.3%) in H-pol and from 5.22 GHz to 5.48 GHz (4.8%) in V-pol at C band. This values reach 7.2% in H-pol and 7.8% in V-pol at X band. In order to show how much the enhancement of gain can be obtained using the proposed PRS, the gain of feed antennas is also presented as the reference in Fig.15. It can be observed that the gain has dramatically improvement, which increases by around 10 dB and 9 dB at lower- and upper- band after the proposed PRS is introduced.

The far-field radiation patterns of the proposed antenna are measured in an indoor anechoic chamber. In our measurement, the co-polar and cross-polar radiation patterns in E- and H-plane at C band in two polarizations have been tested with the operating frequencies of 5.3, 5.35, 5.4, 5.45, 5.5 GHz. At X band, the radiation patterns of the operating frequencies from 9.4 GHz to 9.9 GHz are measured. All the measured results have a good agreement with computed radiation patterns. For brevity, the measured radiation patterns at 5.3 GHz and 9.6 GHz are plotted in Fig.16 and Fig.17, respectively, with the simulated results as comparison. It can be found that the peak radiation happens in the broadside direction at these two frequencies. For H-polarization, the measured sidelobe level is less than -14.5 dB in both of E- and H-planes at 5.3 GHz. Meanwhile, the cross-polarization level is less than -22 dB in the two principal planes. Similar results are obtained in V-polarization at C band, as shown in Fig.17. At upper band, the sidelobe level remains below -14.8 dB and -18.1 dB in the E- and H-plane in the two polarizations. The cross-polarization at 9.6 GHz is very low in E- and H- plane, which are less than -30 dB.

V. Conclusion

A simple low-cost shared-aperture dual-band dual-polarized high gain antenna for SAR applications is presented and studied in this paper. A novel double-layer FSSs are designed as the PRS of FP antennas to create two FP resonate cavities operating at two bands. A simple spare array operating at X band with a single slot-coupled patch operating at C band with dual polarizations are employed as the primary source. The maximum realized gain of this antenna can achieve 16.2 dBi for H-pol, 16.3 dBi for V-pol at C band and 19.8 dBi for H-pol and 19.7 dBi for V-pol at X band. Compared to the conventional dual-band dual-polarized aperture-shared SAR antennas, the proposed antenna has achieved promising performance with very simple feed network and easy fabrication. Such a simple low-cost SAR antenna is very useful for low-cost small satellites.

Acknowledgment

The authors thank the project of 'DIFFERENT' funded by EC FP7 (grant number: 6069923). Thank to Mr. Simon Jakes at the University of Kent for antenna fabrication. Thank to Prof. Raed A.Abd-Alhameed at the University of Bradford for assisting the antenna radiation pattern measurement.

References

[1] W. A. Imbriale, S. Gao, and L. Boccia, *Space antenna handbook: Wiley Online Library*, 2012.

[2] R. L. Jordan, B. L. Huneycutt, and M. Werner, "The SIR-C/X-SAR synthetic aperture radar system," *Geoscience and Remote Sensing, IEEE Transactions on*, vol. 33, pp. 829-839, 1995.

[3] L. L. Shafai, W. A. Chamma, M. Barakat, P. C. Strickland, and G. Seguin, "Dual-band dual-polarized perforated microstrip antennas for SAR applications," *IEEE Trans. Antennas Propag*, vol. 48, pp. 58-66, 2000.

[4] D. M. Pozar and S. D. Targonski, "A shared-aperture dual-band dual-polarized microstrip array," *IEEE Trans. Antennas Propag*, vol. 49, pp. 150-157, 2001.

[5] X. Qu, S. Zhong, Y. Zhang, and W. Wang, "Design of an S/X dual-band dual-polarized microstrip antenna array for SAR applications," *Microwaves, Antennas & Propagation, IET*, vol. 1, pp. 513-517, 2007.

[6] T. D. Sudikila and T. E. Gilles., "Design and Manufacturing of a Dual-band, Dual-polarized and Dual Fed Perforated Array Patch Antenna Pair", *PIERS Proceedings, Moscow*, Russia, August 19, 2012

[7] Pokuls, R., Uher, J., Pozar, D.M.: 'Dual-frequency and dual-polarization microstrip antennas for SAR applications', *IEEE Trans. Antennas Propag*., 1998, 46, (9), pp. 1289–1296

[8] Shi-Gang Zhou, Peng-Khiang Tan, Tan-HuatChio, "Wideband, low profile P- and Ku-band shared aperture antenna with high isolation and low cross-polarisation", *IET Microw. Antennas Propag*., 2013, 7, (4), pp. 223-229.

[9] T. W. Chiou and K. L. Wong, "A compact dual-band dual-polarized patch antenna for 900/1800-MHz cellular systems," *IEEE Trans. Antennas Propag.*, vol. 51, no. 8, pp. 1936–1940, Aug. 2003.

[10] S. Gao, et al., Antennas for modern small satellites, *IEEE Antennas and Propagation Magazine*, Vol. 51, Issue 4, Nov. 2009, pp. 40-56

[11] G. V. Trentini, "Partially reflecting sheet arrays," *Antennas and Propagation, IRE Transactions on*, vol. 4, pp. 666-671, 1956.

[12] N. Wang, Q. Liu, C. Wu, L. Talbi, Q. Zeng, and J. Xu, "Wideband Fabry-Perot Resonator Antenna With Two Complementary FSS Layers," *IEEE Trans. Antennas Propag*, vol. 62, no. 5, pp. 2463-2471, May. 2014.

[13] Young Ju Lee, Junho Yeo, Mittra, R. and Wee Sang Park, "Application of electromagnetic bandgap (EBG) superstrates with controllable defects for a class of patch antennas as spatial angular filters," *IEEE Trans. Antennas Propag*, vol. 53, no. 1, pp. 224- 235, Jan. 2005.

[14] R. Vaidya, R. K. Gupta, S. K. Mishra and J. Mukherjee, "High-gain low side lobe level fabryperot cavity antenna with feed patch array," *Progress In Electromagnetics Research C*, Vol. 28, 223-238, 2012.

[15] Kelly, J.R., Kokkinos, T. and Feresidis, A.P., "Analysis and Design of Sub-Wavelength Resonant Cavity Type 2-D Leaky-Wave Antennas," *IEEE Trans. Antennas Propag*, vol. 56, no. 9, pp. 2817-2825, Sept. 2008.

[16] Y. J. Lee, J. Yeo, R. Mittra, and W. S. Park, "Application of electromagnetic bandgap (EBG) superstrates with controllable defects for a class of patch antennas as spatial angular filters," *IEEE Trans. Antennas Propag*, vol. 53, pp. 224-235, 2005.

[17] Y. Ge, K. P. Esselle, and T. S. Bird, "A method to design dual-band, high-directivity EBG resonator antennas using single-resonant, single-layer

partially reflective surfaces," *Progress In Electromagnetics Research C*, vol. 13, pp. 245-257, 2010.

[18] B. A. Zeb, Y. Ge, K. P. Esselle, Z. Sun, and M. E. Tobar, "A simple dual-band electromagnetic band gap resonator antenna based on inverted reflection phase gradient," *IEEE Trans. Antennas Propag*, vol. 60, pp. 4522-4529, 2012.

[19] A. Pirhadi, M. Hakkak, F. Keshmiri, and R. K. Baee, "Design of compact dual band high directive electromagnetic bandgap (EBG) resonator antenna using artificial magnetic conductor," *IEEE Trans. Antennas Propag*, vol. 55, pp. 1682-1690, 2007.

[20] H. Moghadas, M. Daneshmand, and P. Mousavi, "A dual-band high-gain resonant cavity antenna with orthogonal polarizations," *Antennas and Wireless Propagation Letters, IEEE*, vol. 10, pp. 1220-1223, 2011.

[21] S. Gao and A. Sambell, "Low-cost dual-polarized printed array with broad bandwidth," *IEEE Trans. Antennas Propag*, vol. 52, pp. 3394-3397, 2004.

[22] S. Gao and A. Sambell, "Dual-polarized broad-band microstrip antennas fed by proximity coupling," *IEEE Trans. Antennas Propag*, vol. 53, pp. 526-530, 2005.

[23] R. Gardelli, M. Albani, and F. Capolino, "Array thinning by using antennas in a Fabry-Perot cavity for gain enhancement," *IEEE Trans. Antennas Propag*, vol. 54, pp. 1979-1990, 2006